Lignocellulosic fillers and graphene nanoplatelets as hybrid reinforcement for polylactic acid: effect on mechanical properties and degradability

Roberto Scaffaro*, Andrea Maio*, Emmanuel Fortunato Gulino, Giuseppe Pitarresi

Department of Engineering, University of Palermo, Viale delle Scienze Ed. 6, 90128 Palermo, Italy

* roberto.scaffaro@unipa.it (R.S); andrea.maio@unipa.it (A.M.)

Abstract

This work investigates the effect of adding relatively low amounts of graphene nanoplatelets (GNP) to a biocomposite based on polylactic acid (PLA) and a lignocellulosic filler achieved by grinding *Posidonia Oceanica* leaves (*Posidonia* flour, PF). The ternary composites were prepared by melt extrusion and characterized from a morphological and mechanical point of view. Furthermore, hydrolytic degradation tests were performed under acidic, neutral and alkaline environment up to 900 hours. Density measurements enabled to assess the degree of intraphase, i.e. the capability of polymer macromolecules to enter the voids of PF and a modified Halpin-Tsai model was presented and used to fit experimental data obtained from tensile tests. The results demonstrate that the hybrid reinforcement constituted by GNP and PF allows improving mechanical properties (up to 155%) and speeding up the degradation kinetics with respect to neat PLA and composites loaded with GNP only. In particular, the relatively fast degradation kinetics observed at pH=7 and especially at pH=10 make these hybrid composites very promising in the perspective of marine disposal.

Keywords: Posidonia Oceanica; graphene; hybrid composites; Halpin-Tsai; hydrolytic degradation.

1. Introduction

Biocomposites is a growing area of interest in the field of composite materials, due to the possibility to achieve materials that are fully biodegradable and cost-effective [1–3]. In this context, using agricultural or marine wastes represents an emerging trend in the perspective of developing materials possessing high level of sustainability both from an economic and ecological point of view [1,4]. However, a critical factor associated with manufacturing, application and end-use of biocomposites is the generally observed poor mechanical performance of such materials, as well as the prodegradant activity often exerted by some natural fillers during processing, which may determine further brittleness and may limit the possibility to use them in severe conditions [1,4]. Among the lignocellulosic fillers obtained by marine wastes, *Posidonia* flour (PF), resulting by grinding *Posidonia Oceanica* leaves, shows a promising potential as a filler for polylactic acid (PLA), although it presents the typical drawbacks of lignocellulosic fillers, in terms of poor toughness and pro-degrading effects [1,5–7]. Graphene nanoplatelets (GNP) belong to graphene family, and their use as fillers in PLA-based composites is widespread, due to the possibility to increase breaking properties of PLA and to preserve this polymer from thermal degradation and photo-oxidation, respectively occurring during processing and use [8–15]. Furthermore, while the degradation paths of PLA can be extremely slow, depending on the conditions of degradation tests, with this issue representing an important concern in the case of plastic wastes disposal, recent studies demonstrate the possibility to achieve faster degradation of PLA when loaded with small amounts of GNP [16,17]. Similarly, the typical porous architecture of some lignocellulosic fillers together with their intrinsic hydrophilicity may facilitate water penetration, thus leading to faster degradation kinetics [16–18]. Anyhow, the effect of adding a hybrid reinforcement constituted by nano- and microfillers was marginally investigated in the scientific literature [19–21]. In particular, the effect of adding small amounts of GNP to a green composite based on

PLA and PF have been never reported so far. Aim of this study is to investigate and model the effect of GNP/PF ratio on the mechanical properties of PLA-based composites and to assess eventual changes in the hydrolytic degradation kinetics of such materials in acidic, neutral and alkaline environments. Furthermore, the integration of GNP in PLA/PF systems is expected to enhance stiffness while improving the usually poor breaking properties of such materials.

2. Materials and methods

2.1 Materials

PLA 2002D was purchased by NatureWorks, is an extrusion grade having a content of D-lactic acid monomer equal to ~4%. Graphene nanoplatelets (GNPs), trade name xGnP®, Grade C, were supplied by XG Sciences Inc., Lansing, MI, USA. Each particle consists of several sheets of graphene with an average thickness of approximately 2-5 nm, average diameter between 1 and 2 µm, and a specific surface area of about 750 m^2/g [22–24]. PF, with particle size in the range 150-300 µm, was prepared according to a protocol reported in previous works [1,5].

2.2 Preparation of composites

For the pre-dispersion of nanofillers, GNP (20 g) and PLA (80 g) were poured into 50 g EtOH and subjected to sonication for 90 minutes allowing polymer pellets to be partially swollen and therefore decorated by GNP. Thereafter, diethyl ether was used to remove EtOH and eventual residual solvents were further evaporated at 55 °C *in vacuo* overnight. Different amounts of such PLA-GNP physical mixture were added to fresh PLA and PF, premixed at the solid state, fed to a single-screw extruder (Thermo Scientific Haake Polylab QC) and thereby melt-processed to achieve hybrid nanocomposites at different formulations, listed in **Table 1**. As controls, PLA

containing GNP only or PF only were prepared, too. The temperature profile adopted was: 150-170-180-190 °C. The screw speed was set to 50 rpm. The extrudate was then pelletized and compression-molded (T=190 °C, P=100 bar) into sheets that were cut into specimens of appropriate geometry for further characterizations.

Table 1. Formulations of the samples prepared in the frame of this work

Sample code	PLA	PF	GNP	GNP/PF ratio
PLA	100	0	0	N/A
0.5G	99.5	0	0.5	N/A
1G	99	0	1	N/A
0G10P	90	10	0	0
0.5G10P	89.5	10	0.5	0.05
1G10P	89	10	1	0.1

2.3 Characterization techniques and theoretical modelling

2.3.1 Morphological analysis

Cross-sectional and surface SEM analysis was performed by using an ESEM FEI QUANTA 200. As concerns cross-sectional analysis, specimens were cryo-fractured in liquid nitrogen prior imaging.

2.3.2 Pycnometric density measurements

The real density of PF was measured using helium pycnometer (Pycnomatic ATC from Thermo Electron Corporation). For each sample, ten measurements were carried out and the average value was then recorded. In all the cases, the standard deviations were lower than 0.01 g/cm^3. The porosity was calculated according to Eq. (1) [1,5]:

$$\text{Porosity (\%)} = \left(1 - \rho_{PF,a}/\rho_{PF,r}\right)\cdot 100 \quad (1)$$

Where $\rho_{PF,a}$ and $\rho_{PF,r}$ are PF apparent and real densities, respectively.

The fraction of PF particles filled by PLA (i.e. the percentage of intraphase) was estimated according to Eq. 2 [1,4,5]:

$$Intraphase\ \% = \frac{\rho_{real} - \rho_{unfilled}}{\rho_{filled} - \rho_{unfilled}} \cdot 100 \quad (2)$$

Where ρ_{real} is the density of the composites, ρ_{filled} and $\rho_{unfilled}$ are respectively the theoretical density of the composites considering that all the PF particles are filled by PLA and the theoretical density of the composites considering that none the PF particles are filled by PLA. These two parameters were evaluated according to the following equations (3) and (4):

$$\rho_{filled} = \rho_{PF,r}\,\phi_{PF,r} + \rho_{PLA}\,\phi_{PLA} + \rho_{GNP}\,\phi_{GNP} \quad (3)$$

$$\rho_{unfilled} = \rho_{PF,a}\,\phi_{PF,a} + \rho_{PLA}\,\phi_{PLA} + \rho_{GNP}\,\phi_{GNP} \quad (4)$$

Where $\rho_{PF,r}$ is the density of PF evaluated by pycnometer (i.e. 1.54 g cm^{-3}); $\phi_{PF,r}$ is the volumetric filler fraction in the composites, taking into account this latter density value.

$\rho_{PF,a}$ is the apparent density of PF (i.e. 0.42 g cm^{-3}); $\phi_{PF,a}$ is the volumetric fraction of PF in the composites, taking into account this latter density [1,4,5].

2.3.3 Mechanical characterization

Tensile tests were performed according to ASTM D638–10 standard. Eight specimens for each sample were tested at a crosshead speed of 5 mm/min. Elastic modulus (E) was calculated as the initial slope of each curve, whereas tensile strength (TS) and elongation at break (EB) were measured as the maximum stress and strain values in each stress-strain curve, respectively.

2.3.4 Theoretical modelling of mechanical properties

Experimental results were compared to those theoretically predicted by Halpin-Tsai model, herein modified to take into account the presence of two fillers and a variable

porosity, due to the different ability of macromolecules to form intraphase [1,4,5]. In fact, the well-known Halpin-Tsai model enables predicting the modulus of composites once are known volume fractions of filler and matrix, filler aspect ratio and elastic modulus of the matrix [25].

In a ternary composite, Halpin-Tsai equation can be rewritten as follows [25] (Eq. 5):

$$\frac{E_c}{E_m} = \frac{3}{8}\frac{1+\left(\frac{2w_{GNP}}{3t_{GNP}}\right)\eta_{L,GNP}V_{GNP}+\left(\frac{2w_{PF}}{3t_{PF}}\right)\eta_{L,PF}V_{PF}}{1-\eta_{L,GNP}V_{GNP}-\eta_{L,PF}V_{PF}}+\frac{5}{8}\frac{1+2\eta_{T,GNP}V_{GNP}+2\eta_{T,PF}V_{PF}}{1-\eta_{T,GNP}V_{GNP}-\eta_{T,PF}V_{PF}} \quad (5)$$

Were E_c/E_m is the reduced tensile modulus, expressed as the ratio between the moduli of composite (E_c) and matrix (E_m). Moreover, for both GNP and PF, *w* and *t* respectively indicate the lateral size (under the assumption of width=length) and thickness of particles, η_L and η_T are constants given by [25]:

$$\eta_{L,GNP} = \frac{\left(E_{GNP}/E_m\right)-1}{\left(E_{GNP}/E_m\right)+\left(\frac{2w_{GNP}}{3t_{GNP}}\right)} \quad (6) \qquad \eta_{T,GNP} = \frac{\left(E_{GNP}/E_m\right)-1}{\left(E_{GNP}/E_m\right)+2} \quad (7)$$

$$\eta_{L,PF} = \frac{\left(E_{PF}/E_m\right)-1}{\left(E_{PF}/E_m\right)+\left(\frac{2w_{PF}}{3t_{PF}}\right)} \quad (8) \qquad \eta_{T,PF} = \frac{\left(E_{PF}/E_m\right)-1}{\left(E_{PF}/E_m\right)+2} \quad (9)$$

Of course, the subscripts GNP and PF refer to the type of filler. The intrinsic porosity of PF particles that can be partially filled by polymer macromolecules affects volume fraction of PF and this issue was considered by introducing the volume fraction calculated by considering the real density of the composites, measured by helium pycnometer.

2.3.5 Degradation tests

The degradation tests were carried out by immersing at least three replicates for each sample of disk-shaped specimens, having diameter of 10 mm and thickness of ~2 mm, in three different buffer solutions (pH=4, pH=7 and pH=10) at 37 °C up to 50 days. At predetermined time intervals, the materials were washed thoroughly with distilled water at room temperature, followed by coagulation in diethyl ether and drying under vacuum in oven for 24 hours. After drying, the samples were weighed and the residual weight (W_r) calculated as:

$$W_r\% = \frac{M_t}{M_0} \cdot 100 \qquad (10)$$

Where M_0 and M_t are respectively the initial mass and the mass measured at given time interval [18].

2.3.6 Water contact angle (WCA) measurements

Water contact angle (WCA) measurements were carried out at room temperature by means of FTA 1000 (First Ten Ångstroms, UK) instrument. 4 µL of deionized water were dropped onto the surface of each sample by using an automatic liquid drop dosing system. Images of the drop on the surface were acquired after 20 s.

3. Results and discussion

In **Figure 1 a-d** there are reported the SEM micrographs of cryofractured cross-sections of binary composites, i.e. 0.5G, Fig. 1a, 1G, Fig. 1b, and 0G10P, Figs. 1 c-d. Both 0.5 G and 1G exhibit the absence of PF aggregates and, at least at this scale, no evident macroscopic aggregates of GNP were detected.

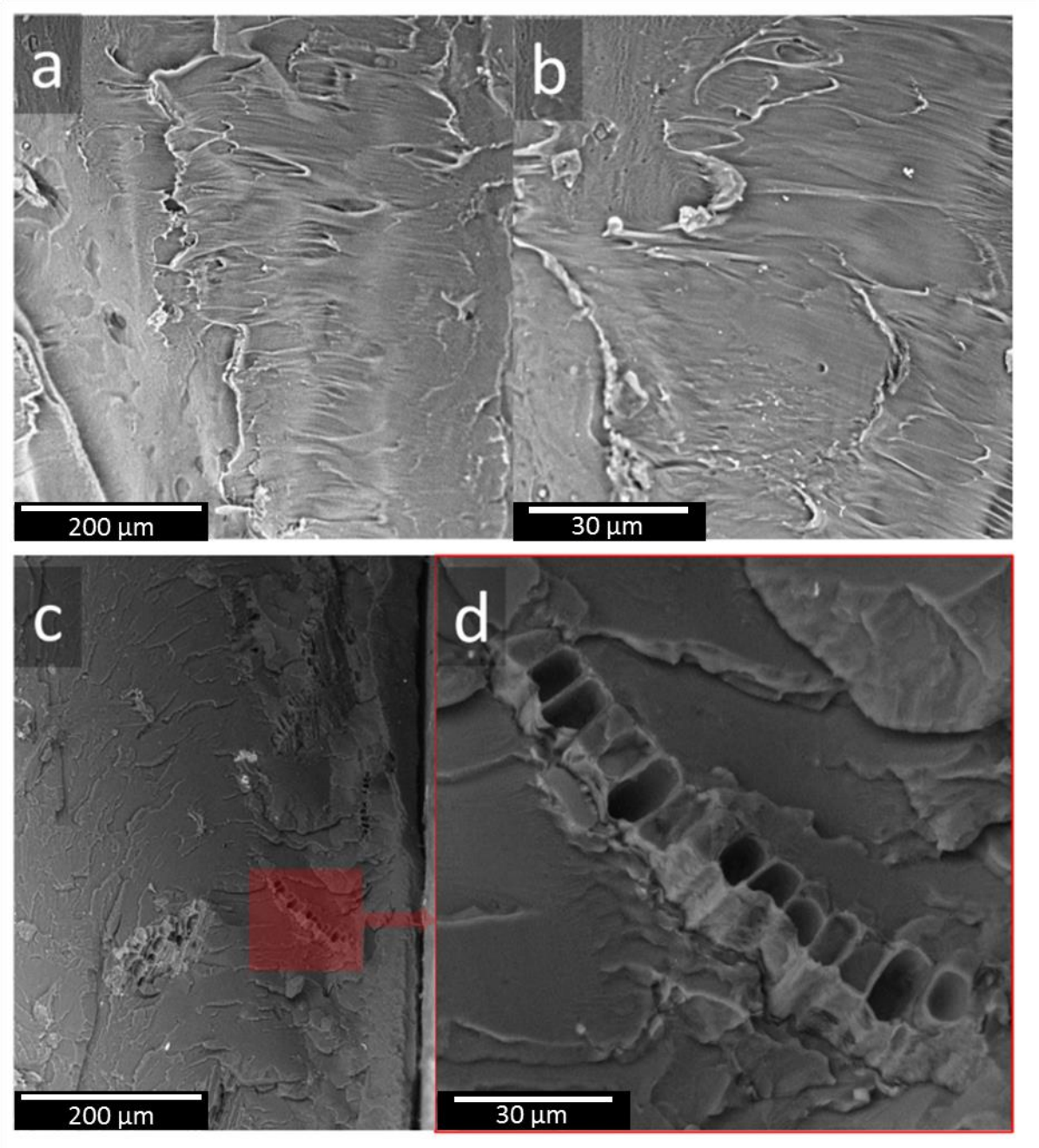

Figure 1. Cross-sectional SEM micrographs of binary composites: 0.5G (a), 1G (b); 0G10P (c-d) at different magnifications (scale bar=200 µm for panels a-c, scale bar=30 µm for panel d).

In the case of 0G10P (Fig. 1c), well-dispersed PF microparticles can be easily recognized and, at higher magnification (Fig. 1d), it is possible to detect the well-known ability of PLA to form intraphase, i.e. to partially fill the empty channels of PF particles, thus giving rise to partially porous composites [1,4,5].

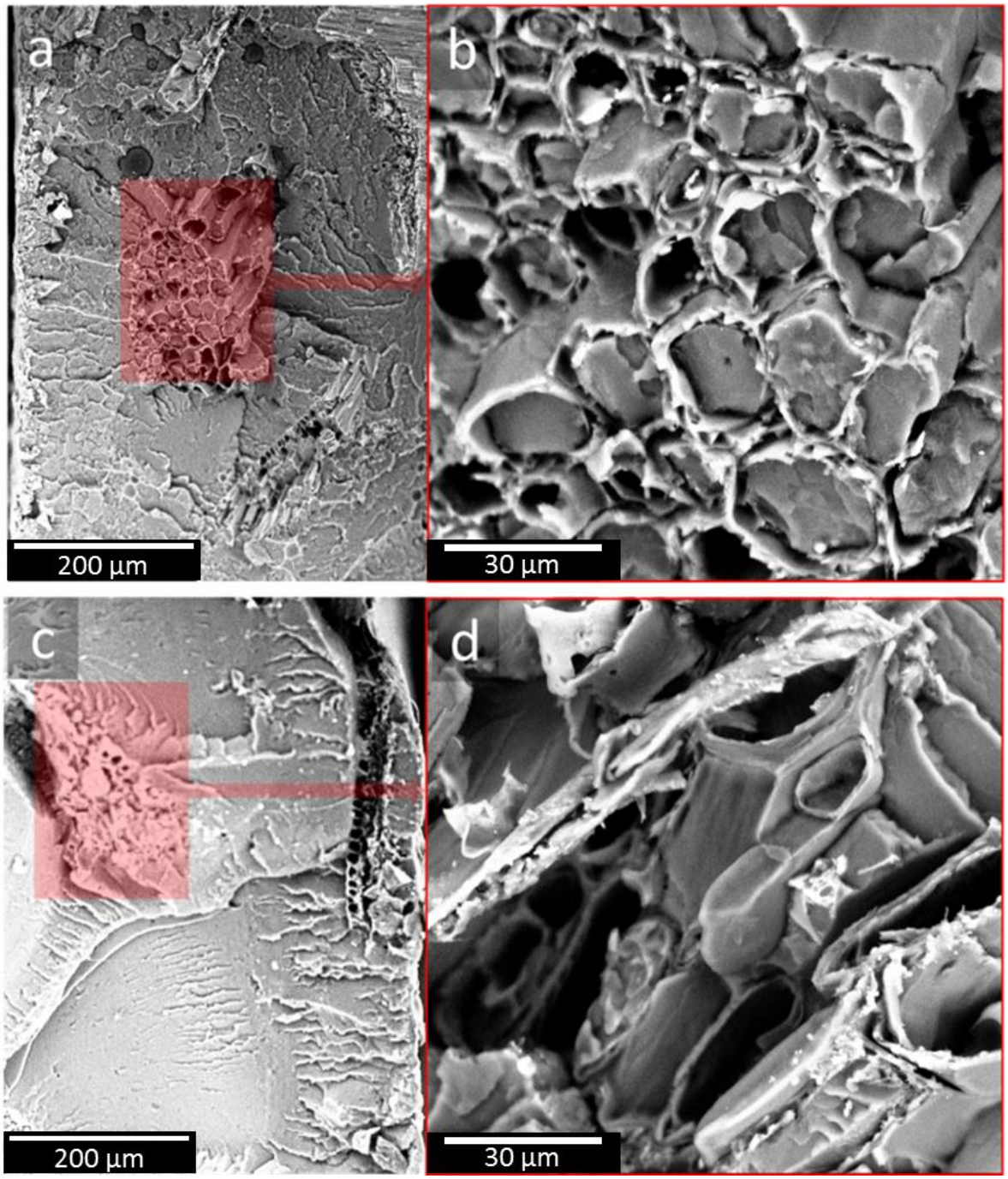

Figure 2. Cross-sectional SEM micrographs of 0.5G10P (a-b) and 1G10P (c-d) at different magnifications (panels a, c: scale bar=200 µm; panels b, d: scale bar=3 µm).

Morphology of ternary composites at different magnifications is provided in **Figure 2** for 0.5G10P (Fig. 2 a-b) and 1G10P (Fig. 2 c-d). Similarly to what observed for 0G10P, even the hybrid composites display a certain tendency of macromolecules to penetrate the pore channels of PF. Aiming to quantitatively assess this parameter, pycnometric analysis was carried out and the intraphase percentage was calculated for all the

formulations and reported in **Figure 3**. The ability of PLA to form intraphase proved to be scarcely affected by the presence of GNP, since 0G10P, 0.5G10P and 1G10P displayed similar values of this property, ranging from 68% (0.5G10P) to 76% (0G10P). Aiming to assess the mechanical properties of the hybrid composites, tensile tests were carried out and the salient results are provided in **Table 2**.

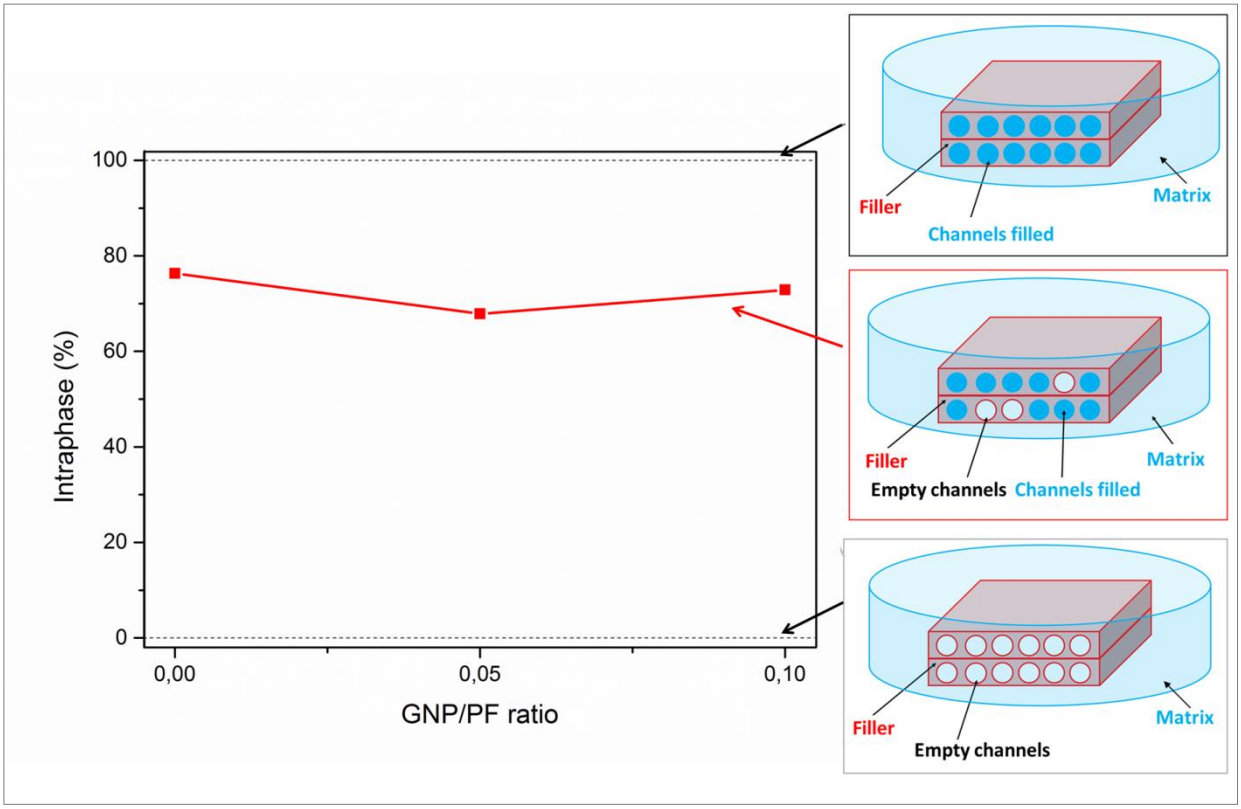

Figure 3. Intraphase calculated according to Eq. (2) as a function of GNP/PF ratio

Table 2. Mechanical properties

Sample	E (MPa)	TS (MPa)	EB (%)
PLA	1800 (±45)	45 (±1.8)	2.5 (±0.1)
0.5G	2262 (±73)	50 (±2.0)	3.1 (±0.2)
1G	2410 (±66)	55 (±1.2)	3.6 (±0.2)
0G10P	1902 (±62)	33 (±2.5)	2.0 (±0.1)
0.5G10P	2400 (±73)	47 (±1.1)	2.6 (±0.1)
1G10P	2820 (±88)	49 (±1.0)	2.7 (±0.2)

Adding GNP determined an increase in elastic modulus from 1800 MPa to 2262 MPa (0.5G) or 2410 MPa (1G), with E_c/E_m values being equal to 1.26 and 1.34, respectively. This stiffness increment is found to be intermediate between that observed in the case of directly melt-mixed GNP and GNP exfoliated into graphene by multi-step approach [10]. Another relevant aspect is that the reinforcing effect of GNP does not follow a linear trend with GNP content, being relatively more prominent at low loading levels, as typically observed in these systems [26–28]. Adding 10 wt.% PF had a moderate influence on PLA stiffness, with an E_c/E_m value close to 1.06. The hybrid composites exhibited E_c/E_m values equal to 1.33 and 1.57, respectively for 0.5G10P and 1G10P. Therefore, hybrid fillers result in composites stiffer than those prepared by adding PF only and GNP only. As regards breaking properties, adding GNP led to higher TS and EB values with increments up to 22% in terms of TS and up to 44% in terms of deformability, whereas adding PF proved to be detrimental to these properties, with decrement observed in TS (~25%) and EB (~20%), being consistent to those observed in previous works [1,4,5,29,30]. The hybrid loading led to composites having TS and EB values intermediate between those containing GNP only and PF only, yet higher than those of neat PLA. This feature is extremely important, since the incorporation of few amounts of GNP may overcome the typical lack of toughness of green composites, which is the most common drawback of this class of materials [1,4,5,29–32]. The experimental results were compared to those predicted by Halpin-Tsai model, herein modified to take into account the presence of two fillers and a certain porosity degree, caused by the porous structure of PF.

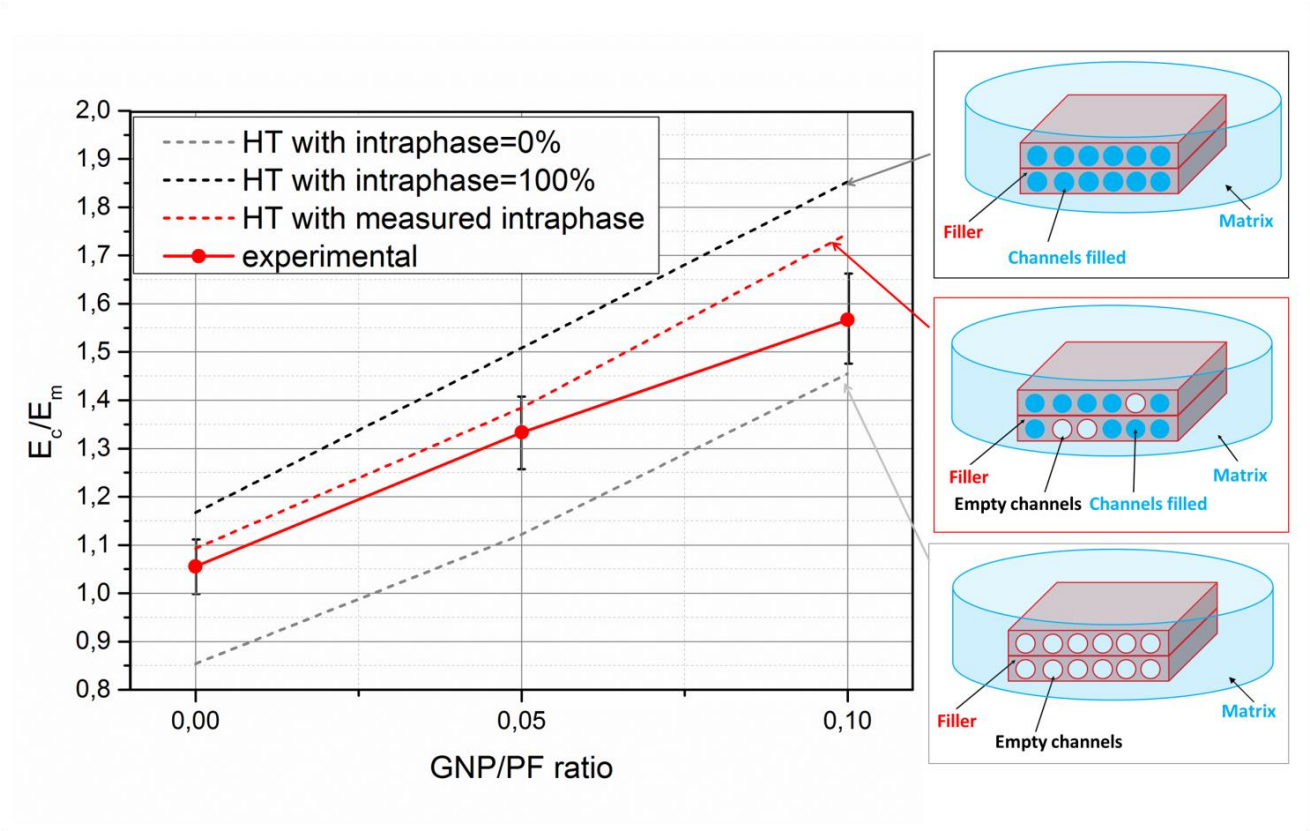

Figure 4. Comparison between values predicted by Halpin–Tsai, considering either limiting cases or measured intraphase, and experimental results of E_c/E_m plotted as a function of GNP/PF ratio.

Figure 4 provides E_c/E_m as a function of GNP/PF ratio experimentally measured, together with the predicted values of Halpin-Tsai in the two limiting cases of intraphase equal to 0% and 100%, as reported in **Table 3**, and in the real case, by using the measured value of interphase obtained by pycnometry, according to Equation 2.

Table 3. Values of volume fraction of GNP and PF, elastic modulus of PF in the two limiting cases

GNP/PF ratio	intraphase 0%			intraphase 100%		
	V_{GNP}	V_{PF}	E_{PF}	V_{GNP}	V_{PF}	E_{PF}
0	0	0.247012	844	0	0.082119	8158.442
0.05	0.002362	0.247464	844	0.002881	0.082302	8158.442
0.1	0.004733	0.247917	844	0.005774	0.082486	8158.442

Basically, the interphase degree affects the volume fraction of fillers in the composites and, of course, the elastic modulus of PF which may vary from 0.84 GPa to 8.45 GPa. As one can see, the corrections made to Halpin-Tsai method by inserting the measured value of intraphase, result in a fairly good fitting of experimental data at lower GNP/PF ratio. However, experimental E_c/E_m proved to be slightly lower than those predicted, which refer to the ideal case of uniform dispersion and perfect adhesion. Degradability is a crucial prerequisite of green materials; therefore, hydrolytic degradation tests of such materials were carried out under three different conditions. As commonly accepted, hydrolytic reactions display pH-dependent kinetics, being particularly faster under alkaline conditions [18]. The degradation determines a dramatic molecular weight reduction and can be easily monitored by mass loss measurements [18,33]. **Figs 5 a-c** report the residual weight fraction of the samples, plotted as a function of immersion time, at pH=4, pH=7 and pH=10, respectively. Regardless of pH, all the samples exhibit an onset of degradation after 24 hours, with ternary composite materials displaying degradation kinetics faster than those of neat PLA at pH=10, while being quite stable at pH=4 and pH=7.

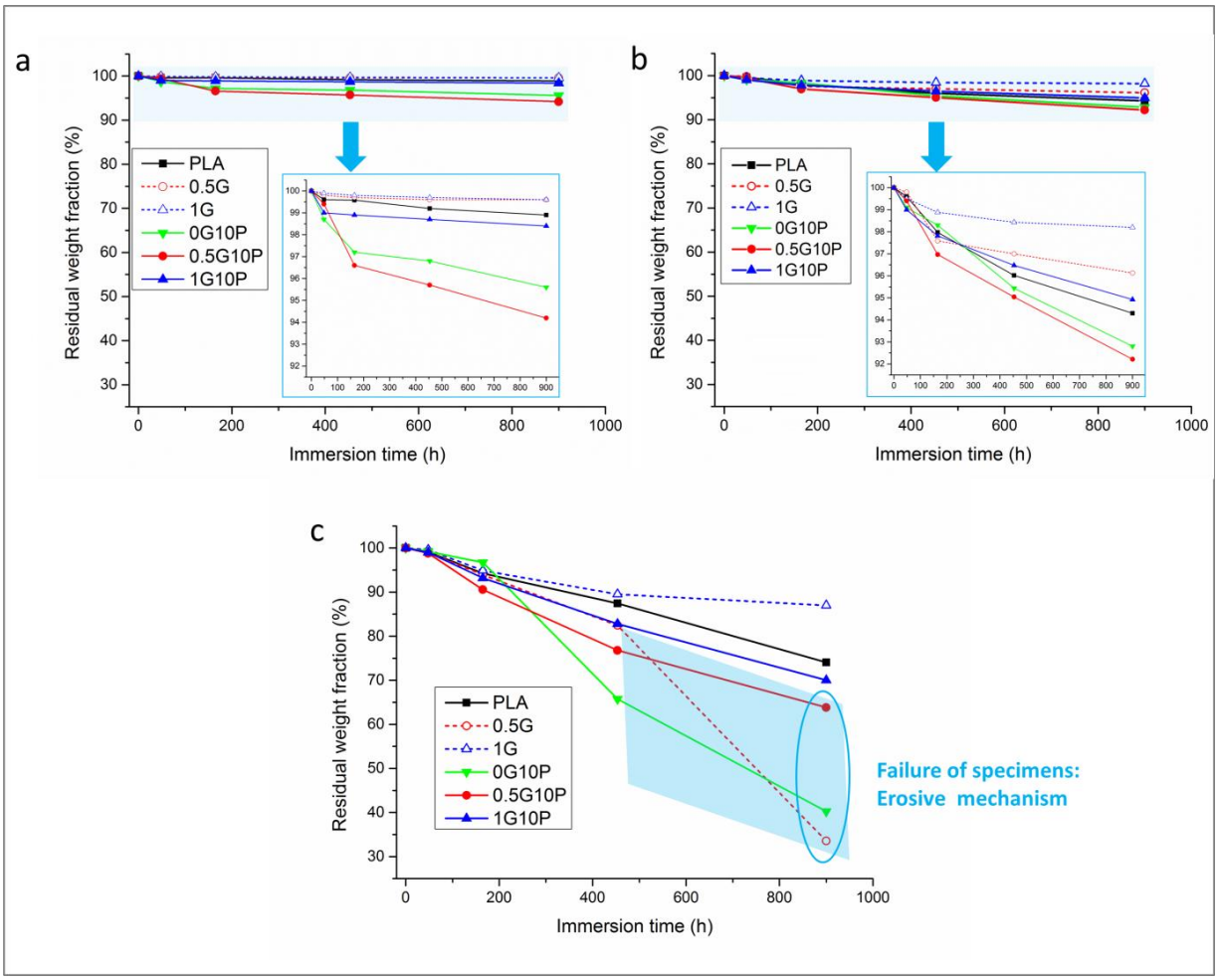

Figure 5. Hydrolytic degradation kinetics at pH=4 (a), pH=7 (b) and pH=10 (c).

Of course, the higher the pH, the higher the degradation extent. At t=450 h, mass loss values were found to be negligible or moderate in the case of pH=4 (up to 4%) and pH=7 (up to 5%, depending on formulation) while being particularly prominent at pH=10, where the mass losses proved to range from 10% to 23%. Interestingly, all the composites - except 1G - display hydrolytic degradation kinetics faster than that of neat PLA. In the case of composites containing GNP only, this feature could be presumably due to the worsening of filler-matrix adhesion caused by the progressive increase of hydrophilicity of the matrix upon degradation time and/or to some role of nanocarbons in activating hydrolytic reactions, while in those containing PF, the porosity of the natural filler, together with the increased hydrophilicity, can reasonably explain the faster kinetics observed [34]. 0.5G10P showed the fastest degradation kinetics at

pH=10. Indeed, 0.510P displayed the lowest intraphase degree, i.e. the highest porosity, with this issue likely playing the main role on the penetration of the solvent throughout the matrix. A possible synergy between GNP and PF in the ratio 0.05 could be even taken into account. At t=453 h, the mass loss of 0.510P is found to be almost 2.5 times higher than that of 1G, which is the less sensitive sample to hydrolytic degradation at all the pH conditions tested. In order to explain these results, it is worth considering that hydrolytic degradation of poly(α-hydroxyl) esters may follow either surface or bulk degradation pathways, with these latter being regulated by diffusive phenomena and kinetics of chemical reactions [33]. Whether the rate of hydrolytic chain scission is faster than that of solvent diffusion into the polymer bulk, the hydrolysis is supposed to occur only at the polymer–liquid interface, thus resulting in the progressive thinning of the sample, whose bulk properties remain unaltered. Otherwise, in the case of water diffusion faster than hydrolytic reactions, hydrolysis should randomly occur throughout the entire polymer bulk. Oligomers and monomers that are formed diffuse out, thus causing gradual erosive phenomena until achieving the equilibrium between diffusion and chemical kinetics. Whether this equilibrium is hindered, the accumulation of -OH and -COOH terminated byproducts may trigger an internal autocatalysis that accelerates the bulk degradation with respect to that of the outer layers [33]. In this case, it would be observed a degraded inner core and a less altered skin until a total hollowing of the structures is achieved. This issue suggests that solvent penetration could be promoted by PF channels. It is worth mentioning that in 0.5G, 0G10P and 0.510P samples, at about 450 hours immersion the failure of specimens occurred, reasonably due to erosive phenomena. This mechanism occurs whether the vitreous core breaks under the compressive tensions exercised by the surrounding swollen gelled zone, as the gel-vitreous interface moves to the nucleus. In this case, the final result will be the quick

formation of multiple gel-solvent interfaces with the progressive disappearance of vitreous regions and the quick acceleration of degradation kinetics.

SEM analysis of samples subjected to hydrolysis was performed in order to get some information about the type of degradation mechanism. Surface SEM micrographs of the samples after 165 hours of hydrolysis at pH=4, pH=7 and pH=10 are reported in **Figs 6-8**. It is possible to detect strong alterations onto the samples surface, as it can be highlighted the insurgence of cracks, whose size is strictly correlated to the pH level: the higher the alkalinity the larger the cracks [35]. At pH=4, Fig.6, all the samples display an unaltered surface morphology, except for 0G10P and 0.5G10P, which showed micrometric holes and increased roughness. Neat PLA shows a practically unaltered surface at pH=4 (Fig. 6a) and pH=7 (Fig. 7a), while the formation of small cracks was detected at pH=10 (Fig. 8a). The effect of the formulation on the surface etching during hydrolysis is quite evident, since it can be observed that low amounts of GNP determines faster cracking (Figs 7b-8b), while at 1% GNP the hydrophobicity of surface somehow resulted in a stronger resistance toward degradation (panels c of the same Figures). Indeed, graphene was found to either promote or hinder degradability of PLA, depending on filler concentration, processing technique adopted and pH of the environment [16,17]. GNPs may delay hydrolytic reactions whether they are able to form a barrier thus reducing the moisture diffusion into the polymer matrix, and this feature occurs as the filler content is adequate to block the solvent penetration [36]. Otherwise, their addition may result in faster degradation rates, since the presence of voids or defects facilitates water diffusion within PLA and subsequent degradation [17]. It is worth considering that hydrophilicity of PLA progressively increases upon degradation time and this issue may determine a worsening in filler-matrix adhesion, as above discussed [34]. Interestingly, a sort of phase separation can be observed in 0.5G samples, whereas 1G showed a more uniform structure. 0G10P displays surface

cracking only at pH=10. Hybrid loading leads to interesting results: regardless of formulation, when GNP and PF are used together, hybrid composites display the conspicuous formation of cracks, with these latter ones propagating in proximity of PF microparticles (Figs 6-8 d-f).

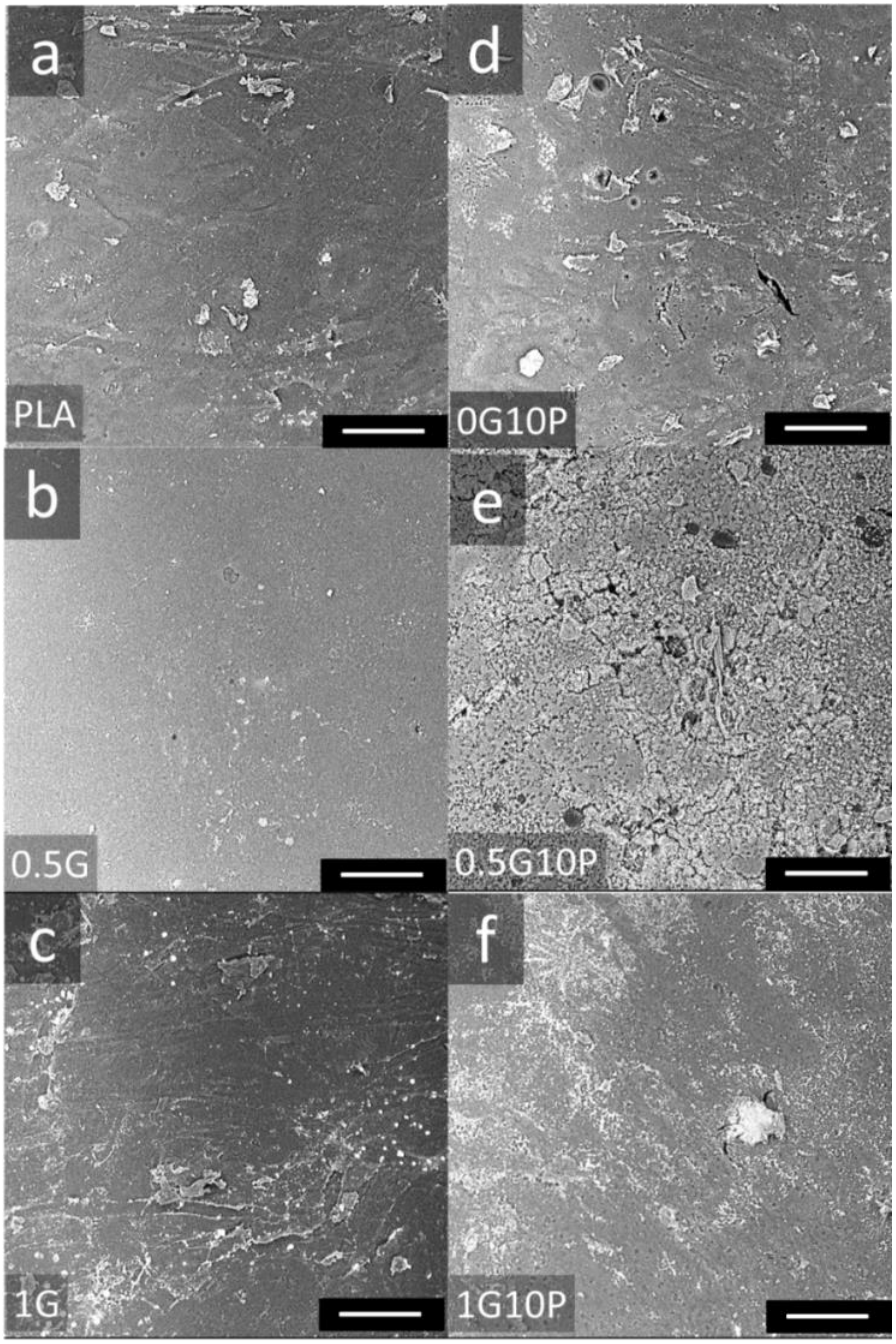

Figure 6. Surface SEM micrographs of samples immersed for 165 hours at pH=4 (scale bar=100 μm)

As previously discussed, 0.5G, 0G10P and 0.5G10P samples experienced a failure after about 450 hours immersion at pH=10, with a quick acceleration of degradation kinetics. Indeed, by comparing surface morphology of 0G10P (Fig. 8d) and 1G10P (Fig. 8f), the larger extent of cracking phenomena was detected for 1G10P, which retained 70% of its initial weight at the end of experiment, whereas 0G10P, although displaying less cracking phenomena, underwent failure with a more dramatic mass loss. This issue suggests that degradation pathways may have followed different mechanisms, depending on formulation.

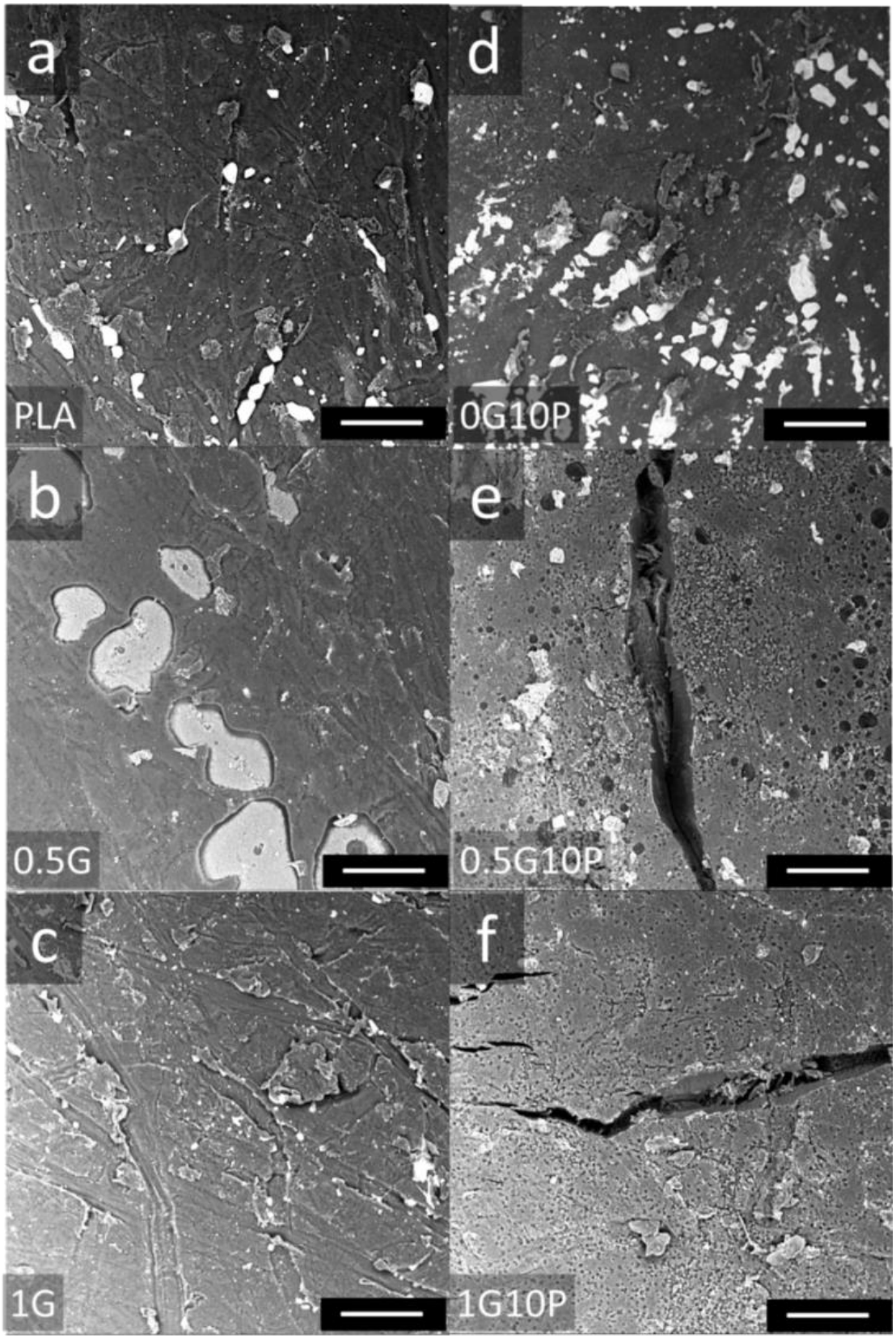

Figure 7. Surface SEM micrographs of samples immersed for 165 hours at pH=7 (scale bar=100 μm)

In fact, based on the results collected, it can be hypothesized that the addition of PF and low content of GNP determine the prevalence of swelling phenomena owing to the solvent penetration inside the structure, thus leading to faster degradation kinetics with respect to neat PLA, 1G and 1G10P whose degradation seems to follow a purely surface pathway, likely due to a hydrolytic degradation faster than solution penetration [33].

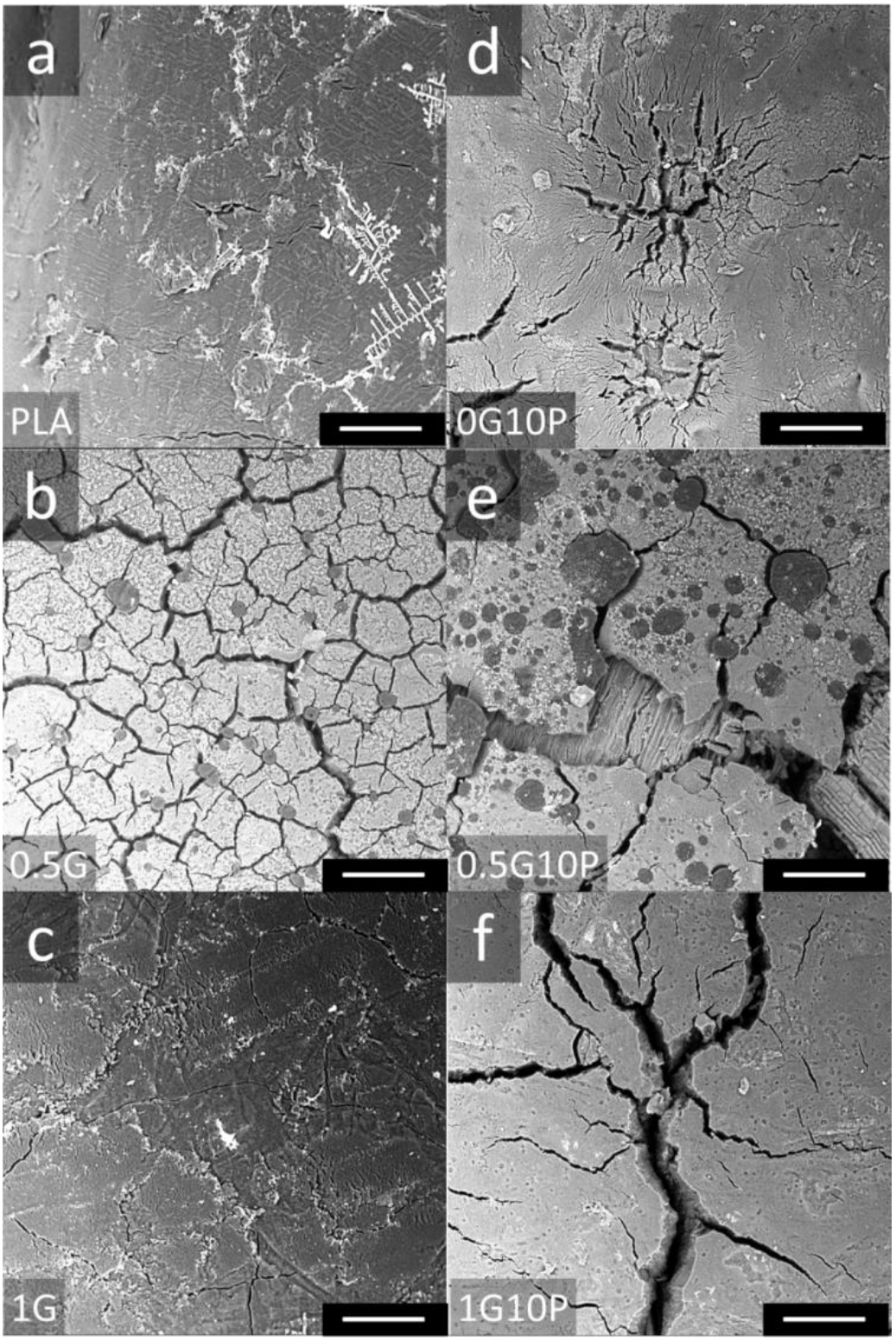

Figure 8. Surface SEM micrographs of samples immersed for 165 hours at pH=10 (scale bar=100 μm)

Aiming to get further insight this phenomenon, WCA measurements were carried out before and after hydrolytic tests and the results are provided in **Table 4**. As predictable, adding GNP determines a progressive decrease of wettability, with WCA going from

74° (for neat PLA) to 88° (0.5G) and 114 ° (1G). By contrast, incorporating hydrophilic PF led to an increase of wettability with WCA decreasing to 59°.

For samples containing hybrid fillers, WCA proved to be the resultant of the two opposite contributions of GNP and PF. In 0.5G10P, hydrophilic character of PF prevailed on the hydrophobicity of GNP and, before the experiment, WCA was equal to 68° (i.e. less than that of PLA), otherwise for 1G10P, the content of GNP was enough to counterbalance the hydrophilicity of PF and WCA was equal to 86°, that is more hydrophobic than PLA and much similar to that of 0.5 G.

Table 4. WCA measured before and after degradation tests

Sample code	**WCA_0**	**$WCA_{900,\ pH=4}$**	**$WCA_{900,\ pH=7}$**	**$WCA_{900,\ pH=10}$**
PLA	74	70	34	31
0.5G	88	85	54	N/A*
1G	114	96	70	16
0G10P	59	50	50	N/A*
0.5G10P	68	48	52	N/A*
1G10P	86	77	56	35

* specimens broken

The initial values of WCA may be responsible for the solvent penetration at the beginning of experiment. As the degradation pathways are ongoing, the hydrolytic scissions determine an increase of polar moieties with ensuing enhancement of wettability [37]. Moreover, as envisaged by SEM analysis, the degraded samples displayed an increased roughness, which is known to further affect wettability [38]. In fact, although it cannot be found any close relationship between WCA and mass retention of each sample, all the samples that underwent hydrolytic tests, regardless of pH, proved to show WCA values lower than those of untreated samples. For each sample, it can be easily detected the effect of pH, since the higher the pH, the lower the WCA, with this aspect being particularly prominent for the materials treated in alkaline environment that displayed WCA values generally lower than those treated at pH=4 and pH=7. At pH=4, negligible differences were observed in terms of WCA values at the

end of experiment, with this feature being consistent with the little variations displayed by the samples in terms of weight and morphology. In some cases, the results of WCA were not found in full agreement with the outcomes of residual weight measurements. In fact, after 900 hours treatment at pH=10, 1G showed the highest mass retention (close to 90%) but the lowest WCA value (16°), whereas PLA and 1G10P proved to retain 70-75% of their initial weight, while showing WCA values equal to 31° and 35°, respectively. This feature, in fully agreement with the results of mass retention tests and SEM analysis, suggests that the degradation mechanism of these samples may differ each other. In 1G sample, the presence of GNP may have hindered the propagation of degradation pathways into the bulk, whereas in 1G10P the presence of hydrophilic, porous PF may have promoted solvent penetration, thus enhancing the contact area of specimens exposed to degradative phenomena.

In order to summarize the degradation pathways of PLA in the different systems prepared in the frame of this work, a schematics is provided in **Figure 9**.

Fig. 9a reports the general hydrolytic degradation mechanism of PLA chains.

The results of WCA, mass loss tests and morphological analysis likely suggest that neat PLA underwent a prevalent surface degradation, Fig. 9b.

As regards 0G10P and 0.5G, Figs. 9 c-d, respectively, the results above discussed indicated that for such systems bulk/erosive degradation became more relevant, likely due to the penetration of solution in the sample core. Obviously, this occurrence may favor the propagation of hydrolytic chain scissions into the bulk.

For 0G10P, Fig. 9c, the solution penetration is reasonably driven by both the intrinsic hydrophilicity and porosity of PF fillers. Differently, in 0.5G (Fig. 9d), it can be hypothesized that degradation induced the formation of polar moieties in the polymer

(see again Fig. 9a), thus progressively enhancing hydrophilicity while worsening PLA-GNP adhesion with consequent formation of cracks and microchannels that allowed the solution to propagate into the bulk.

At high GNP content (1G, Fig. 9e) a hydrophobic surface barrier due to the abundance of GNP reasonably hindered the penetration of the solution.

Of course, in the case of hybrid reinforcement, the degradation behaviour depends on the synergistic or antagonistic effect of GNP content and PF. In particular, at low GNP content (0G10P) a synergistic interaction between hydrophilic PF and GNP was observed (combination of the effects represented in panels c and e), while at higher GNP contents (1G10P), the formation of hydrophobic graphenic barriers partially counterbalanced hydrophilic PF.

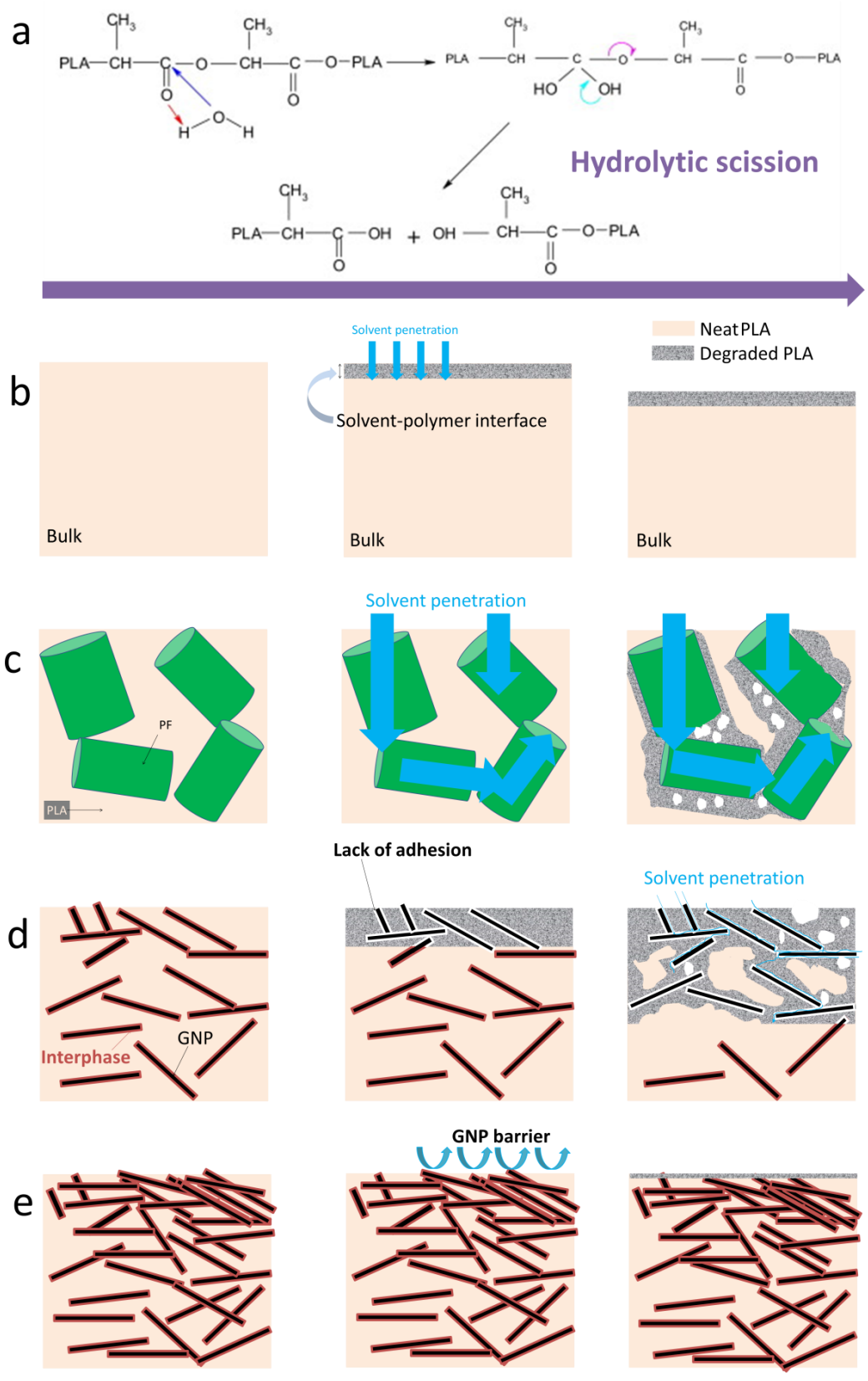

Figure 9. Schematics of hydrolytic scission mechanism of PLA (a) and pictorial representation of degradation pathways propagation in neat PLA (b), 0G10P (c), 0.5G (d), 1G (e).

4. Conclusions

The effect of incorporating 0.5 wt.% or 1 wt.% GNP to a biocomposite constituted by PLA and 10 wt.% *Posidonia Oceanica* flour (PF) was assessed, by monitoring eventual changes in morphology, mechanical properties and hydrolytic degradability.

The morphological analysis highlighted that both filler were well-dispersed in PLA matrix and that the polymer was able to partially fill empty channels of PF.

The results of mechanical tests clearly evidenced that hybrid reinforcement allows enhancing mechanical properties of green composites, and a monotonic increase of stiffness was observed as a function of GNP content, with relative increments up to +55%. Furthermore, experimental data can be adequately predicted by a modified Halpin-Tsai model that takes into account the presence of two different fillers and the porosity of PF. Moreover, the presence of GNP allowed enhancing tensile strength and elongation at break up to +48% and +35%, thus hindering the typical embrittlement of green composites loaded with natural fillers.

As concerns degradation tests, all the samples, regardless of formulation, displayed negligible or moderate changes when treated for 900 hours at pH=4 and pH=7, with mass losses below 8%, while showing remarkable weight losses (up to 70%) at pH=10. Hydrolytic degradation behavior of hybrid composites proved to depend on GNP loading level. In fact, at low GNP content, the presence of discontinuities at PLA/PF and PLA/GNP interfaces had strong repercussions on the hydrolytic degradation behavior of such hybrid composites, whose kinetics proved to be much faster than that of neat PLA, owing to a better capability of the solvent to penetrate the structure, with ensuing swelling phenomena that governed the hydrolysis pathways in ternary composites, until leading to the failure of specimens. At high GNP content, instead, the barrier effect of hydrophobic nanocarbons partially counterbalanced the hydrophilicity

of lignocellulosic fillers, thus resulting in slower degradation kinetics, although faster than those of neat PLA. Upon adjusting formulation, it is possible modulating degradation kinetics of such materials, whose mass loss values were found to vary from 1% to 8% and from 30% to 70% after 900 hours immersion in neutral and alkaline environment, respectively.

References

[1] R. Scaffaro, A. Maio, F. Lopresti, Physical properties of green composites based on poly-lactic acid or Mater-Bi® filled with Posidonia Oceanica leaves, Compos. Part A Appl. Sci. Manuf. 112 (2018) 315–327. doi:https://doi.org/10.1016/j.compositesa.2018.06.024.

[2] I. Benito-González, A. López-Rubio, M. Martínez-Sanz, Potential of lignocellulosic fractions from Posidonia oceanica to improve barrier and mechanical properties of bio-based packaging materials, Int. J. Biol. Macromol. 118 (2018) 542–551. doi:https://doi.org/10.1016/j.ijbiomac.2018.06.052.

[3] W. Liu, L.T. Drzal, A.K. Mohanty, M. Misra, Influence of processing methods and fiber length on physical properties of kenaf fiber reinforced soy based biocomposites, Compos. Part B Eng. 38 (2007) 352–359. doi:https://doi.org/10.1016/j.compositesb.2006.05.003.

[4] R. Scaffaro, A. Maio, E.F. Gulino, B. Megna, Structure-property relationship of PLA-Opuntia Ficus Indica biocomposites, Compos. Part B Eng. 167 (2019) 199–206. doi:https://doi.org/10.1016/j.compositesb.2018.12.025.

[5] R. Scaffaro, F. Lopresti, L. Botta, PLA based biocomposites reinforced with Posidonia oceanica leaves, Compos. Part B Eng. 139 (2018) 1–11. doi:https://doi.org/10.1016/j.compositesb.2017.11.048.

[6] F. Luzi, E. Fortunati, D. Puglia, R. Petrucci, J.M. Kenny, L. Torre, Study of disintegrability in compost and enzymatic degradation of PLA and PLA nanocomposites reinforced with cellulose nanocrystals extracted from Posidonia Oceanica, Polym. Degrad. Stab. 121 (2015) 105–115. doi:10.1016/j.polymdegradstab.2015.08.016.

[7] B. Ferrero, T. Boronat, R. Moriana, O. Fenollar, R. Balart, Green composites based on wheat gluten matrix and posidonia oceanica waste fibers as reinforcements, Polym. Compos. 34 (2013) 1663–1669. doi:10.1002/pc.22567.

[8] L. Botta, R. Scaffaro, F. Sutera, M.C. Mistretta, Reprocessing of PLA/graphene nanoplatelets nanocomposites, Polymers (Basel). 10 (2018). doi:10.3390/polym10010018.

[9] R. Scaffaro, A. Maio, Influence of Oxidation Level of Graphene Oxide on the Mechanical Performance and Photo-Oxidation Resistance of a Polyamide 6, Polymers (Basel). 11 (2019). doi:10.3390/polym11050857.

[10] R. Scaffaro, A. Maio, Integrated ternary bionanocomposites with superior

mechanical performance via the synergistic role of graphene and plasma treated carbon nanotubes, Compos. Part B Eng. 168 (2019) 550–559. doi:https://doi.org/10.1016/j.compositesb.2019.03.076.

[11] C. Gonçalves, I.C. Gonçalves, F.D. Magalhães, A.M. Pinto, Poly(lactic acid) Composites Containing Carbon-Based Nanomaterials: A Review, Polymers (Basel). 9 (2017). doi:10.3390/polym9070269.

[12] R. Scaffaro, A. Maio, G. Lo Re, A. Parisi, A. Busacca, Advanced piezoresistive sensor achieved by amphiphilic nanointerfaces of graphene oxide and biodegradable polymer blends, Compos. Sci. Technol. 156 (2018) 166–176. doi:https://doi.org/10.1016/j.compscitech.2018.01.008.

[13] R. Kotsilkova, I. Petrova-Doycheva, D. Menseidov, E. Ivanov, A. Paddubskaya, P. Kuzhir, Exploring thermal annealing and graphene-carbon nanotube additives to enhance crystallinity, thermal, electrical and tensile properties of aged poly(lactic) acid-based filament for 3D printing, Compos. Sci. Technol. 181 (2019). doi:10.1016/j.compscitech.2019.107712.

[14] C. Liu, S. Ye, J. Feng, Promoting the dispersion of graphene and crystallization of poly (lactic acid) with a freezing-dried graphene/PEG masterbatch, Compos. Sci. Technol. 144 (2017) 215–222. doi:https://doi.org/10.1016/j.compscitech.2017.03.031.

[15] A. Maio, R. Scaffaro, L. Lentini, A. Palumbo Piccionello, I. Pibiri, Perfluorocarbons–graphene oxide nanoplatforms as biocompatible oxygen reservoirs, Chem. Eng. J. 334 (2018) 54–65. doi:10.1016/j.cej.2017.10.032.

[16] A. Bher, I.U. Unalan, R. Auras, M. Rubino, C.E. Schvezov, Graphene modifies the biodegradation of poly(lactic acid)-thermoplastic cassava starch reactive blend films, Polym. Degrad. Stab. 164 (2019) 187–197. doi:https://doi.org/10.1016/j.polymdegradstab.2019.04.014.

[17] A.M. Pinto, C. Gonçalves, I.C. Gonçalves, F.D. Magalhães, Effect of biodegradation on thermo-mechanical properties and biocompatibility of poly(lactic acid)/graphene nanoplatelets composites, Eur. Polym. J. 85 (2016) 431–444. doi:https://doi.org/10.1016/j.eurpolymj.2016.10.046.

[18] L. Wan, C. Li, C. Sun, S. Zhou, Y. Zhang, Conceiving a feasible degradation model of polylactic acid-based composites through hydrolysis study to polylactic acid/wood flour/polymethyl methacrylate, Compos. Sci. Technol. 181 (2019). doi:10.1016/j.compscitech.2019.06.002.

[19] C.I. Idumah, A. Hassan, S. Bourbigot, Influence of exfoliated graphene nanoplatelets on flame retardancy of kenaf flour polypropylene hybrid nanocomposites, J. Anal. Appl. Pyrolysis. 123 (2017) 65–72. doi:https://doi.org/10.1016/j.jaap.2017.01.006.

[20] S. Sheshmani, A. Ashori, M.A. Fashapoyeh, Wood plastic composite using graphene nanoplatelets, Int. J. Biol. Macromol. 58 (2013) 1–6. doi:https://doi.org/10.1016/j.ijbiomac.2013.03.047.

[21] H. Essabir, R. Boujmal, M.O. Bensalah, D. Rodrigue, R. Bouhfid, A. el kacem Qaiss, Mechanical and thermal properties of hybrid composites: Oil-palm fiber/clay reinforced high density polyethylene, Mech. Mater. 98 (2016) 36–43. doi:https://doi.org/10.1016/j.mechmat.2016.04.008.

[22] R. Scaffaro, L. Botta, A. Maio, M.C. Mistretta, F.P. La Mantia, Effect of Graphene Nanoplatelets on the Physical and Antimicrobial Properties of Biopolymer-Based Nanocomposites, Materials (Basel). 9 (2016) 351. doi:10.3390/ma9050351.

[23] R. Scaffaro, L. Botta, A. Maio, G. Gallo, PLA graphene nanoplatelets nanocomposites: Physical properties and release kinetics of an antimicrobial agent, Compos. Part B Eng. 109 (2017) 139–146. doi:http://dx.doi.org/10.1016/j.compositesb.2016.10.058.

[24] R. Scaffaro, A. Maio, L. Botta, E.F. Gulino, D. Gulli, Tunable release of Chlorhexidine from Polycaprolactone-based filaments containing graphene nanoplatelets, Eur. Polym. J. 110 (2019) 221–232. doi:10.1016/j.eurpolymj.2018.11.031.

[25] W. Li, A. Dichiara, J. Bai, Carbon nanotube–graphene nanoplatelet hybrids as high-performance multifunctional reinforcements in epoxy composites, Compos. Sci. Technol. 74 (2013) 221–227. doi:https://doi.org/10.1016/j.compscitech.2012.11.015.

[26] Y. Gao, O.T. Picot, E. Bilotti, T. Peijs, Influence of filler size on the properties of poly(lactic acid) (PLA)/graphene nanoplatelet (GNP) nanocomposites, Eur. Polym. J. 86 (2017) 117–131. doi:https://doi.org/10.1016/j.eurpolymj.2016.10.045.

[27] A.M. Pinto, J. Cabral, D.A.P. Tanaka, A.M. Mendes, F.D. Magalhães, Effect of incorporation of graphene oxide and graphene nanoplatelets on mechanical and gas permeability properties of poly(lactic acid) films, Polym. Int. 62 (2013) 33–40. doi:10.1002/pi.4290.

[28] R. Scaffaro, A. Maio, F. Lopresti, Effect of graphene and fabrication technique on the release kinetics of carvacrol from polylactic acid, Compos. Sci. Technol. 169 (2019). doi:10.1016/j.compscitech.2018.11.003.

[29] M.E. Malainine, M. Mahrouz, A. Dufresne, Lignocellulosic flour from cladodes of Opuntia ficus-indica reinforced poly(propylene) composites, Macromol. Mater. Eng. 289 (2004) 855–863. doi:10.1002/mame.200400103.

[30] M. Seggiani, P. Cinelli, N. Mallegni, E. Balestri, M. Puccini, S. Vitolo, C. Lardicci, A. Lazzeri, New Bio-Composites Based on Polyhydroxyalkanoates and Posidonia oceanica Fibres for Applications in a Marine Environment, Materials (Basel). 10 (2017).

[31] M. Morreale, R. Scaffaro, A. Maio, F.P. La Mantia, Mechanical behaviour of Mater-Bi/wood flour composites: A statistical approach, Compos. Part A Appl. Sci. Manuf. 39 (2008) 1537–1546. doi:10.1016/j.compositesa.2008.05.015.

[32] M. Morreale, R. Scaffaro, A. Maio, F.P. La Mantia, Effect of adding wood flour to the physical properties of a biodegradable polymer, Compos. Part A Appl. Sci. Manuf. 39 (2008) 503–513. doi:http://dx.doi.org/10.1016/j.compositesa.2007.12.002.

[33] R. Scaffaro, A. Maio, F. Sutera, E.F. Gulino, M. Morreale, Degradation and Recycling of Films Based on Biodegradable Polymers: A Short Review, Polymers (Basel). 11 (2019). doi:10.3390/polym11040651.

[34] Y.Z. Wan, Y.L. Wang, X.H. Xu, Q.Y. Li, In vitro degradation behavior of carbon fiber-reinforced PLA composites and influence of interfacial adhesion strength, J. Appl. Polym. Sci. 82 (2001) 150–158. doi:10.1002/app.1834.

[35] R. Scaffaro, F. Sutera, L. Botta, Biopolymeric bilayer films produced by co-extrusion film blowing, Polym. Test. 65 (2018) 35–43. doi:https://doi.org/10.1016/j.polymertesting.2017.11.010.

[36] A. Finniss, S. Agarwal, R. Gupta, Retarding hydrolytic degradation of polylactic acid: Effect of induced crystallinity and graphene addition, J. Appl. Polym. Sci. 133 (2016). doi:10.1002/app.44166.

[37] A. Pellis, E.H. Acero, H. Weber, M. Obersriebnig, R. Breinbauer, E. Srebotnik, G.M. Guebitz, Biocatalyzed approach for the surface functionalization of poly(L-lactic acid) films using hydrolytic enzymes, Biotechnol. J. 10 (2015) 1739–1749. doi:10.1002/biot.201500074.

[38] M. Zou, S. Beckford, R. Wei, C. Ellis, G. Hatton, M.A. Miller, Effects of surface roughness and energy on ice adhesion strength, Appl. Surf. Sci. 257 (2011) 3786–3792. doi:https://doi.org/10.1016/j.apsusc.2010.11.149.

Declaration of interests

□ The authors declare that they have no known competing financial interests or personal relationships that could have appeared to influence the work reported in this paper.

□The authors declare the following financial interests/personal relationships which may be considered as potential competing interests:

Roberto Scaffaro: Conceptualization, Methodology, Supervision, Formal Analysis, Data Curation, Writing-Reviewing and Editing, Resources, Project administration.

Andrea Maio: Conceptualization, Investigation, Methodology, Formal analysis, Software, Visualization, Data Curation, Writing-Reviewing and Editing, Writing-Original draft preparation.

Emmanuel F Gulino: Investigation, Visualization, Data Curation, Software.

Giuseppe Pitarresi: Investigation, Formal Analysis, Supervision.